SPH Simulations of Abrasive Processes at a Microscopic Scale

Christian Nutto, Claas Bierwisch, Hanna Lagger, Michael Moseler
MikroTribologie Centrum μTC, Fraunhofer IWM
Freiburg, Germany
christian.nutto@iwm.fraunhofer.de

***Abstract*—We present the development of smoothed particle hydrodynamics (SPH) simulations for the investigation of the industrial application of abrasive flow machining (AFM). This process cannot be observed in-situ in experiments and therefore demands for numerical simulations at a grain-size process scale.**

There are only a few numerical models available for the AFM process, which are strongly simplified. In order to optimize the machining, an explicit approach of including individual grains in the abrasive suspension is essential. These grains are simulated by individual clusters of SPH particles, which are integrated in time by a rigid body solver.

For the correct force transmission between the suspended abrasive particle and the workpiece, a realistic representation of the stress in the fluid model of the suspension is necessary. Therefore, the rheology of the fluids, containing the abrasive grains, has been experimentally characterized. Since the tested suspensions show a viscoelastic behavior, we have employed a viscoelastic fluid model and have used experimentally gathered data for the calibration of the applied numerical model. The abrasive process on a workpiece and the removal of material from its surface is modeled by the Johnson-Cook ductile flow stress model in combination with a strain-based failure criterion.

We show that the particle method can reproduce key aspects for the simulation of the process of abrasive flow machining. By the application of the Johnson-Cook model, we are able to determine wear contacts between solid materials on a microscopic scale.

I. Introduction

Abrasive flow machining (AFM) is a widely applied industrial manufacturing technique for technical materials and components, which rely on the precise finishing of surfaces in order to achieve their designated performance. It is usually applied for technical components exhibiting complex geometries. However, obtaining the necessary surface roughness and a sufficiently high material removal rate in the finishing process of hard-to-access surfaces remains a great challenge. The abrasive process itself consists of cutting, burring, and surface polishing at a microscopic level. The complex interaction at the wear contact between the fluid, the abrasive particle, and the technical component cause great difficulties in optimizing the process parameters for satisfying results.

The AFM process is usually applied for the finishing of complex internal geometries. Depending on the geometrical size of the inlet and the internal structure, fluids of different viscosities are applied. For inlets and structures with a small cross section fluids of low viscosity are used, while for larger geometries highly viscous and viscoelastic polymeric fluid media are applied. Together with the embedded abrasive grains, this suspension is forced to flow along the internal contours of a technical component. The relative motion of the abrasive medium and the workpiece at contact then causes the wear of material. The aim of optimizing the process parameters for a given workpiece in industrial applications is usually only achieved by trial-and-error. The difficulties to adjust the parameters correctly for a cost efficient finishing of each technical component prevents its utilization in a greater variety of industrial applications despite its huge range of application.

Numerical investigations possess a great possibility to study the process of AFM at a microscopic level. However, there are only a few physical models available and the applied models are strongly simplified, e.g., abrasive grains are considered to be homogeneous, therefore neglecting their individual structure. Until now, there are no numerical simulations available that take into account the individual grain characteristics and their highly dynamic interactions with the workpiece and the fluid at the instant of the wear contact. However, in order to optimize the wear of the material, an explicit approach of including individual particles in the abrasive suspension is promising.

The long term goal of this work is to study numerically the process of abrasive flow machining at a scale where the actual interaction between the abrasive grain and the technical component occurs. Knowing the interaction at the grain size scale, we intend to develop analytical models for the removal rate at the length-scale of the workpiece. This would allow to derive process parameters and to design suspensions with specific abrasive characteristics for a given industrial application. Our goal is to develop numerical tools and models that include the precise coupling between various viscous and viscoelastic polymeric suspensions, the abrasive grains and the technical component.

In section II, we will shortly review the underlying physical models and the SPH framework applied in our numerical approach. Section II-A introduces the concept of viscoelastic media and their numerical approximation. Plasticity models and a fatigue failure criterion is discussed in section II-B. Section III compares the numerical methods to analytical or experimentally gathered data. A short example of a simulation

of an abrasive flow machining process at the microscopic scale is given in section IV. A short summary of the results is given in section V.

II. Governing Equations

The simulation of precise microscoping finishing of surfaces in AFM processes rely on several key aspects. The applied abrasive medium usually consists of a viscoelastic suspension. The process of microcutting due to microsized abrasive particle needs the consideration of plasticity. Removal of material is described by a damage criterion, which determines a fatigue material failure under large strains. In the following, we will discuss the implementation of each of these important aspects for the simulation of the microscopic processes of AFM.

A. Viscoelastic model

Depending on the time scale of a dynamical process, viscoelastic media can be more viscous or more elastic, therefore showing properties of liquid and solid bodies. In the literature there are many examples of viscoelastic models. In [1], we have already presented the implementation of the most basic, linear viscoelastic model — the Oldroyd-B model. Here, we present the implementation of a viscoelastic constitutive equation given by Phan-Thien & Tanner [2], referred to as the PTT model. This viscoelastic model is usually employed for highly concentrated solutions and for polymer melts.

For a simple isothermal flow of a viscoelastic fluid, the equation of motion can be written as

$$\frac{\mathrm{D}v^\alpha}{\mathrm{D}t} = \frac{1}{\rho}\frac{\partial \sigma^{\alpha\beta}}{\partial x^\beta} + F^\alpha \,, \tag{1}$$

where ρ describes the fluid density, v^α the αth component of the fluid velocity, and $\sigma^{\alpha\beta}$ is the (α,β)th component of the Cauchy stress tensor. F^α contains any other volume forces on the fluid. The independent variables are the spatial coordinates, x^β, and the time, t. $\mathrm{D}/\mathrm{D}t$ is the material derivative. In the following we employ the Einstein summation convention, i.e., the summation is carried out over repeated indices.

The Cauchy stress tensor can be split in two different terms:

$$\sigma^{\alpha\beta} = -p\delta^{\alpha\beta} + \tau^{\alpha\beta} \,, \tag{2}$$

where p is the pressure, and δ denotes the Kronecker symbol with $\delta^{\alpha\beta} = 0$ if $\alpha \neq \beta$ and $\delta^{\alpha\beta} = 1$ if $\alpha = \beta$. This requires a constitutive equation, which relates the additional stress term, τ, to the fluid dynamical properties. In order to attain viscoelastic behavior, we employ the PTT fluid model [2]:

$$f(\mathrm{tr}(\underline{\tau}))\tau^{\alpha\beta} + \lambda \overset{\triangledown}{\tau^{\alpha\beta}} = 2\eta d^{\alpha\beta} \,, \tag{3}$$

where $\overset{\triangledown}{\tau^{\alpha\beta}}$ denotes the upper convected derivative defined by

$$\overset{\triangledown}{\tau^{\alpha\beta}} = \frac{\mathrm{D}\tau^{\alpha\beta}}{\mathrm{D}t} - \frac{\partial v^\alpha}{\partial x^\gamma}\tau^{\gamma\beta} - \frac{\partial v^\beta}{\partial x^\gamma}\tau^{\alpha\gamma} \,. \tag{4}$$

The rate-of-strain tensor, d, is given by

$$d^{\alpha\beta} = \frac{\partial v^\alpha}{\partial x^\beta} + \frac{\partial v^\beta}{\partial x^\alpha} \,. \tag{5}$$

The coefficient function

$$f(\mathrm{tr}(\underline{\tau})) = 1 + \frac{\lambda\epsilon}{\eta}\tau^{\alpha\alpha} \tag{6}$$

determines the fracturing of polymeric chains under high dynamical loads as well as shear-thinning effects. The characteristic parameter are the relaxation time, λ, the elongation parameter, ϵ, and the viscosity, η.

Equation (3) expresses the constitutive equation for viscoelastic material showing only one specific relaxation time, λ. However, realistic viscoelastic media are more heterogenous and usually possess a continuous spectrum of relaxation times [3]. As an approximation to the realistic viscoelastic media, (3) can be rewritten as a constitutive equation for a discrete number N of deviatoric stresses, τ_i, with a corresponding relaxation time, λ_i, and viscosity, η_i. The complete deviatoric stress tensor, τ, is then given by the sum of the single stress components:

$$\tau = \textstyle\sum_i^N \tau_i \tag{7}$$

$$f(\mathrm{tr}(\underline{\tau}_i))\tau_i^{\alpha\beta} + \lambda_i \overset{\triangledown}{\tau_i^{\alpha\beta}} = 2\eta d^{\alpha\beta} \,. \tag{8}$$

In order to close the system of equations one needs to define a relationship between the pressure and the density. We approximate the incompressible fluids with the weakly compressible approach

$$p(\rho) = \frac{c^2\rho^2}{2\rho_0} \,, \tag{9}$$

where ρ is the local density, ρ_0 is the reference density, and c is the speed of sound. The density variation, $\delta\rho/\delta\rho_0$, is proportional to the squared Mach number, M^2 ($M \equiv v/c$), where v is a typical velocity of the simulated process. Thus with an appropriate choice for the value of the sound speed, one can control the density variation within 1%, which is a valid approximation for incompressible fluids [4].

In case of solid materials, a Gruneisen equation-of-state (EOS) was used in order to define the relationship between the pressure and the density change. The parameters for the Gruneisen EOS were taken from [5].

B. Plasticity and failure models

1) Plastic deformations: Abrasive processes, as they occur in AFM, depend on the physical interaction between two solid materials. The generated forces by the interaction may induce non-reversible surface defects and may induce residual stresses within the materials that may lead to a fatigue failure. For the correct numerical treatment of abrasive processes such as microcutting and deburring, the occurring stresses and high strains at the interaction interface of the solids need to be transferred into accumulated material damage.

Two main processes are responsible for material damage in AFM. For high strains and strain-rates the material is deformed plastically. If the plastic deformation reaches a material dependent strain limit, the material undergoes fatigue failure and material can be removed from the surface.

A (MPa)	B (Mpa)	C	n	m
324	114	0.002	0.42	1.34

TABLE I
JOHNSON-COOK YIELD MODEL PARAMETERS FOR AL6061-T6 FROM [7]

For the numerical treatment of plastic deformations we have implemented a plasticity model based on a modified Johnson-Cook model [6]

$$\tau_{\rm eq} = [A + B\epsilon^n][1 + \dot{\epsilon}^*]^C[1 - T^{*m}]\,. \qquad (10)$$

which describes the yield point in dependence of the plastic strain, ϵ, and strain-rate, $\dot{\epsilon}^*$, where $\dot{\epsilon}^* = \dot{\epsilon}/\dot{\epsilon}_0$ is a dimensionless strain-rate and $\dot{\epsilon}_0$ is a user defined reference strain-rate. The homologous temperature, T^*, is a function of process temperature, T, melting temperature, $T_{\rm m}$, and reference temperature, T_0, typically the room temperature,

$$T^* = \frac{T - T_0}{T_m - T_0}\,. \qquad (11)$$

The quantity A is here the initial yield stress, and the other quantities, B, C, n, and m are material dependent and experimentally determined parameters, which describe strain and strain-rate hardening, as well as softening of materials by a considerable temperature increase.

For the numerical treatment of the temperture during the wear contact of the solids, it is assumed that due to the short time scale of the interaction, heat conduction can be neglected and the process behaves in an adiabatic manner. We imply that 95% of the hereby conducted plastic work, W_p, due to the plastic strain is converted into heat,

$$T - T_0 = \frac{0.95 W_{\rm p}}{\rho_o C_{\rm p}}\,, \qquad (12)$$

where ρ_0 and $C_{\rm p}$ are the density and the specific heat of the target material, respectively. The rest of the energy is stored in defects of the microscopic structure of the material.

The top panel of Fig. 1 shows a snapshot of a simulation employing the plasticity model described above. A grain-shaped particle is shot at an aluminium target at a speed of 300 m/s with an incident angle of 60°. The interaction between the impactor and the target material has already occurred and the target has been deformed plastically. The impactor is modelled as ideally hard and is not affected by the impact. The process itself can be phenomenologically described as a microploughing of the impactor through the target resulting in a plastically deformed kerf with a pile up of material at the end of the groove. The applied parameters can be found in Table I.

2) Ductile failure model: The model described in Sect. II-B1 describes solely plastic deformations without the capability to model any removal of material. In order to treat chip formation and separation, an additional criteria is necessary, which describes the occurrence of fatigue material failure of the damaged workpiece under dynamical workload. For this purpose we have implemented a ductile Johnson-Cook based failure criterion [7]

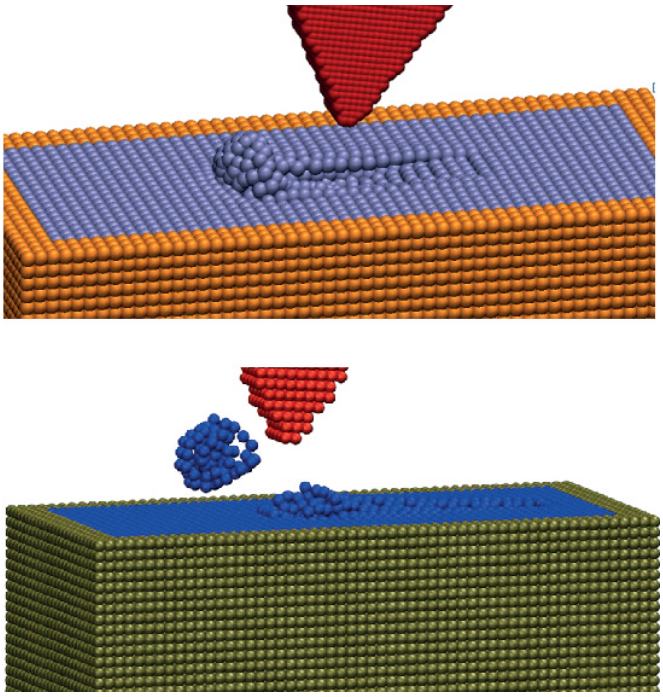

Fig. 1. *Top panel:* snapshot of a simulation of a grain impacting an aluminium target. The deformations are described by a Johson-Cook plasticity model. *Lower panel:* same simulation but with the application of a failure criterion for large plastic strains.

$$D = \frac{\sum \Delta\epsilon_{\rm p}}{\epsilon_{\rm f}}\,, \qquad (13)$$

which is used in combination with the plastic yield model described above. The failure strength, D, considers the added up plastic deformations, $\Delta\epsilon_{\rm p}$. As soon as the failure strength reaches a value $D \geq 1$ the material fails and the tensile stress is set to zero. The failure strain, $\epsilon_{\rm f}$, is determined by [6]

$$\epsilon_{\rm f} = [D_1 + D_2 \exp(D_3\tau^*)][1 + \dot{\epsilon}^*]^{D_4}[1 + D_5 T^*]\,, \qquad (14)$$

where the Johnson-Cook parameters, D_i, are determined experimentally for the target material [8]. The quantity τ^* is the stress triaxiality ratio defined by $\tau^* = \tau_{\rm H}/\tau_{\rm eq}$, where $\tau_{\rm H}$ and $\tau_{\rm eq}$ are the hydrostatic pressure and the yield stress, respectively.

The lower panel of Fig. 1 displays a snapshot of the same simulation setup as the top panel with the exception of the application of a ductile failure model. Again, the snapshot is taken just after the impactor has penetrated the aluminium workpiece. Now, due to the implementation of a failure model, chip formation can occur and material can be removed from the surface of the workpiece. Plastically deformed material remains due to the microploughing effect of the impacting grain within and on the side of the groove. The applied Johnson-Cook parameter can be found in Table II.

Johnson-Cook parameters	D_1	D_2	D_3	D_4	D_5
Values	-0.77	1.45	-0.47	0	1.60

TABLE II
JOHNSON-COOK FAILURE MODEL PARAMETERS FOR AL6061-T6 FROM [7]

III. COMPARISON BETWEEN EXPERIMENT AND NUMERICAL MODELS

For the realistic simulation of abrasive flow machining, the models described above need be to calibrated with experimental results or analytical models.

A. Calibration of the viscoelastic model

Viscoelastic fluids can be characterized by two distinctive quantities, viz., the storage modulus, G', and the loss modulus, G'' [9]. The storage modulus is a measure for the deformation energy stored in the fluid sample during a shear process. After the load is removed, this energy acts as a restoring force trying to recover the initial condition of the fluid and compensate the obtained deformation. Thus, the storage modulus represents the elastic part of the fluid. In contrary, the loss modulus determines how much energy is dissipated during the process of deformation, e.g. due to structural changes or frictional heating.

In principle, both characteristic properties can be measured with oscillation rheometers. A simplified version of this test can be explained by a Two-Plates-Model. The experimental setup consists of a bottom plate, which is stationary, and a upper plate, which is forced to oscillate by a varying shear force. The sample initially rests within the gap between both plates. The motion of the upper plate causes a shearing of the sample and a shear stress is imposed on the fluid. The temporal behavior between the imposed deflection of the sample, $\gamma(t) = \gamma_A \sin(\omega t)$, and the resulting shear stress, $\tau(t) = \tau_A \sin(\omega t + \delta)$, is characteristic for the viscoelastic behavior, where γ_A and τ_A are the amplitude of the deflection and the stress, respectively. The viscoelastic behavior can be measured by the phase shift, δ, between the imposed deflection and the stress. For fluid samples that show ideally viscous behavior, there is a phase delay between the deflection and stress of $\delta = 90°$. For ideally elastic behavior, the deflection and the resulting stress are in phase, $\delta = 0°$. Viscoelasticity is the regime between both ideal cases. Thus, measuring the phase relation between the deformation and the stress, one can determine the storage, G', and loss modulus, G'', by

$$G' = (\tau_A/\gamma_A) \cdot \cos\delta \quad (15)$$

$$G'' = (\tau_A/\gamma_A) \cdot \sin\delta\,. \quad (16)$$

The numerical realization of oscillation rheology can be achieved by the implementation of Lees-Edwards boundary conditions [10] as a numerical approach to a shear cell. By this, we do not consider the whole experimental setup but a small portion of the fluid sample at the location of shear symmetry. Instead of imposing a continuous steady shear upon the fluid sample, we apply oscillating boundary conditions at the bottom and upper boundary of the simulation domain. In the horizontal direction we use periodic boundary conditions. The two dimensional computational domain of the numerical fluid sample has an spatial extent of 1 cm by 1 cm. It is resolved by 100 SPH particles, placed on a 10 by 10 regular grid.

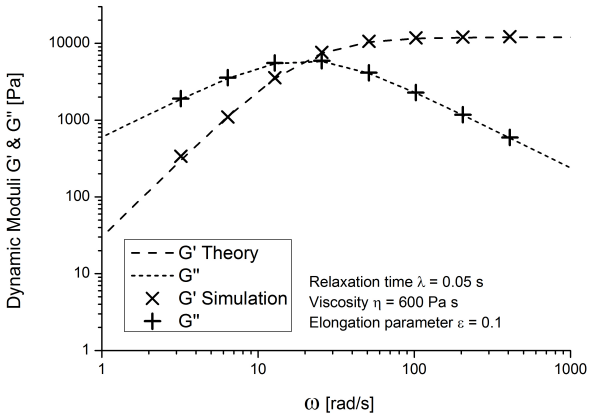

Fig. 2. Comparison between numerical and analytical viscoelastic model. The solid lines describe the analytical Maxwell model for the storage and loss modulus. The points are the numerically derived values for the PTT model for the same set of parameters as indicated within the figure.

Inflicting a certain deformation, $\gamma(t)$, on the sample, the simulation then yields the stress, $\tau(t)$, as a function of time containing a possible phase shift with respect to the applied deformation. The two modulus G' and G'' can be determined by a fit of the function

$$\tau(t) = G'\gamma_A \sin(\omega t) + G''\gamma_A \cos(\omega t) \quad (17)$$

to the recorded stress curve, $\tau(t)$, with G' and G'' as the fitting parameters and γ_A given as the amplitude of deformation.

In our simulations, we carried out a frequency sweep while keeping the deformation amplitude of the oscillation constant at $\gamma = 0.05\%$. These tests can be used for a quantitative description of the viscoelastic behavior of the PTT fluid model and the calibration of the parameter space.

In Fig. 2 the result of a numerical frequency sweep using the PTT model for one set of arbitrary parameters is shown. The solid lines represent the analytical solution of the storage and loss modulus for a single viscoelastic Maxwell mode with the same set of parameters. The analytical viscoelastic moduli are determined by

$$G'(\omega) = G_\mathrm{p} + \sum_{i=1}^{N} G_i \frac{\omega^2\lambda_i^2}{1+\omega^2\lambda_i^2}\,, \quad (18)$$

$$G''(\omega) = \sum_{i=1}^{N} G_i \frac{\omega\lambda_i}{1+\omega^2\lambda_i^2}\,, \quad (19)$$

where N determines the number of different parameter sets for the relaxation time, λ_i, and viscosity, η_i. For a single set of

Mode	1	2	3	4	5
λ_i [s]	0.002	0.02	0.5	2	5
η_i [Pa s]	15	40	738	756	17315

TABLE III
PARAMETERS OF THE VISCOELASTIC MULTI-MODE PTT MODEL.

parameters, as shown in Fig. 2, $N = 1$. G_p is a constant value for the storage modulus. The consistency between analytical model and numerically derived values demonstrates that the viscoelastic constitutive equation (3) represents very well the behavior of the viscoelastic approximation of the Maxwell model.

However, as mentioned before, realistic media are more heterogeneous and possess more than one single set of parameters, i.e,. more than one relaxation time. Thus, in order to calibrate the numerical data for realistic viscoelastic media, one can do a least square fit of (18) to either the experimentally derived storage or the loss modulus. In our case we choose to fit the storage modulus to an experimental data set of the realistic abrasive flow media MF20 since it shows a gel-like behavior, i.e. the storage modulus is solely larger than the loss modulus. The result of the fit and the comparison to the experimentally gathered data is presented in Fig. 3. For the calibration of the numerical model and the reconstruction of the realistic storage modulus a set of five different parameters is necessary, which are listed in Table III.

For the numerical reconstruction of the loss modulus, an additional calibration method is necessary since the material does not behave strictly as a Maxwell material and shows a more viscous behavior, i.e. a larger storage modulus, than the analytical Maxwell model. For the calibration of the viscous phase, we apply the Cross viscosity law which is a function of the shear rate and hence of the oscillation frequency.

By the use of the presented calibration procedure, a numerical description of realistic viscoelastic media is possible as is demonstrated in Fig. 3.

B. *Validation of plasticity model*

Similar to the calibration of the viscoelastic media it is necessary to check the predictability of the plasticity model for the simulations of the AFM processes. For this, we compare numerical simulations to an analytical solution of an impact experiment.

The setup consists of a hard glass sphere with a diameter of 600 μm shot vertically at a surface of a plane parallel target. The target is made of 100Cr6 steel and has the outline of a square box with the dimension of 800 μm in the x- and y-direction and a depth of 400 μm in the z-direction. At the lower bound, the box is supported by a particle layer which is held fixed in space during the simulation. The side walls and the top side of the box can evolve freely under the impact of the glas sphere. The resolution of the particle spacing is 15 μm. The impact velocities are 40 m/s, 60 m/s, and 80 m/s, and 100 m/s.

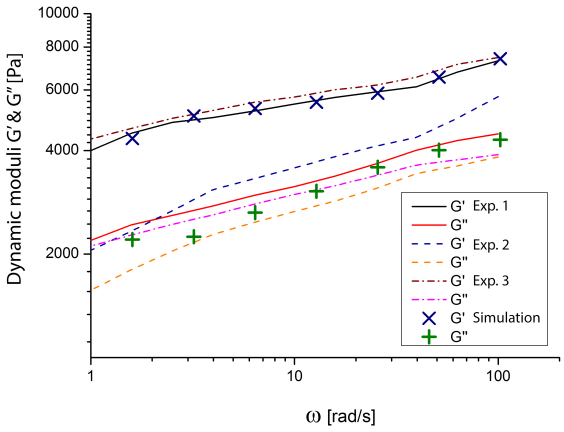

Fig. 3. Comparison between numerically derived storage and loss moduli for the multi-mode PTT model and the experimentally derived values for three independent measurements.

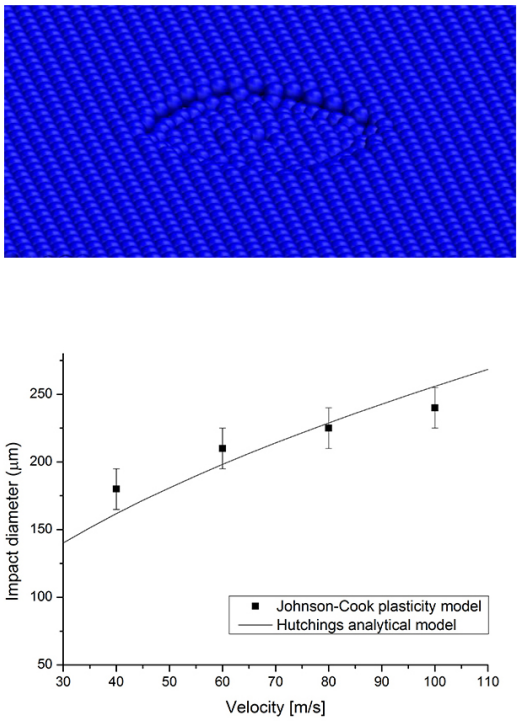

Fig. 4. *Top panel:* deformation region just after the rebound of the sphere. The deformation region is 400 μm in diameter and corresponds to an impact velocity of 100 m/s. *Lower panel:* comparison of the numerically derived impact diameters as a function of impact velocity with the analytical model from Hutchings.

The upper panel of Fig. 4 displays a snapshot of the simulation just after the rebound of the sphere from the target for an impact velocity of 100 m/s. The impact crater can be best recognized in the plastic deformation that has occurred during the event of the impact and which can be used to measure the diameter of the crater and compare it to the analytical expression for the impact diameter, d, as a function

of impact velocity [11]

$$d = 2\,r\,\sqrt{2v}\left(\frac{2\rho}{3H}\right)^{1/4}, \qquad (20)$$

where r is the radius of the impacting sphere, v is the impact velocity, ρ and H are the density and the hardness of the target, respectively. The lower panel of Fig. 4 shows the comparison of the derived diameters of the simulation and the analytically determined values. Within the errors, the numerically determined diameters fit very well to the analytical solution.

IV. Simulation of a microscopic abrasive flow process

With the validation of both, the viscoelastic and plasticity models, we are confident that we can apply our numerical schemes to the simulation of the process of abrasive flow machining on a microscopic level. For this, we focus on the abrasive interaction of an ideally hard grain with an edge of a fixed workpiece within a flow field of a newtonian fluid inside a channel. The numerical setup of the investigation is shown in the top panel of Fig. 5. The dimension of the computational domain is 300 μm by 130 μm in the x- and y-direction, respectively, and 170 μm in height in the z-direction. In the y-direction, we apply periodic boundary conditions. The resolution of the particle spacing is 5 μm. The top and bottom of the computational domain is constrained by a three particle thick wall of fixed particles defining the outline of the channel. The newtonian fluid with a viscosity of $\eta = 5$ Pa s is forced to flow through the channel by a body force acting solely on the fluid. Within the fluid, we have placed an idealistic abrasive spherical particle with a diameter of 50 μm, which is dragged along with the fluid motion. Towards the end of the channel, a workpiece consisting of aluminium is placed within the channel. Although it is held fixed in space within the channel by a supporting wall at the backside of the workpiece, the particles of the workpiece may be deformed by a possible interaction with the abrasive grain. The Johnson-Cook parameters are the same as in section II-B.

The middle panel of Fig 5 shows a snapshot of the simulation when the abrasive particle forms a wear contact with the edge of the workpiece. The fluid motion forces the spherical particle to be dragged over the edge of the workpiece, where eventually, material of the edge is plastically deformed and some of the material is removed.

The lower panel displays a snapshot where the particle has just passed the edge of the workpiece and the wear contact is dissolved. A deburring of the workpiece edge due to the plastic deformation is clearly discernible. There are also a few particles that have been removed from the edge due to the imposed large strains by the abrasive particle. After the particle has passed the edge, it does not form another wear contact with the workpiece.

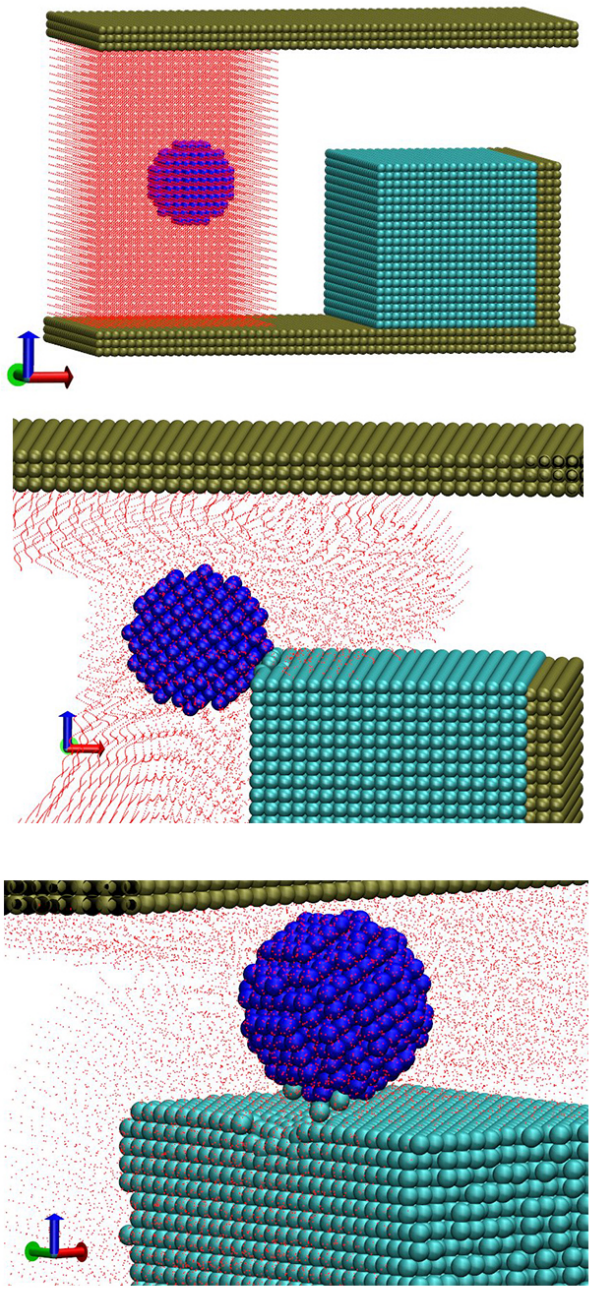

Fig. 5. *Top panel:* initial setup of the microscopic abrasive flow machining simulation, where the red dots represent the fluid, the blue sphere is the abrasive particle placed inside fluid matrix, the turqoise particles belong to the workpiece fixed inside the channel, which is supported by the walls of the channel plotted in a greenish color. *Middle panel:* snapshot of the simulation when the particle forms a wear contact with the edge of the workpiece. *Lower panel:* snapshot after the abrasive particle has been dragged over the edge of the workpiece by the fluid. A deburring of the workpiece edge due to the plastic deformations and the removal of material is cleary discernible.

V. Summary

For our aim to numerically study the process of abrasive flow machining on a microscopic scale, we have outlined the necessary steps that need to be taken in order to incorporate the different physical effects that occur during the process.

In a first step, a viscoelastic model has to be considered that takes the viscoelastic nature of the applied abrasive media into account that are used in AFM processes. A comparison with an analytical model demonstrated that the applied numerical scheme is capable of reproducing theoretical results. For the calibration with a realistic AFM fluid medium, a multi-mode PTT model is necessary in order to reproduce the realistic storage and loss modulus.

For the plastic deformations and material removal we have implemented a Johnson-Cook plasticity model and a failure criterion based on the integrated plastic deformations in order to consider the effects of microploughing and microcutting during the formation of a wear contact. The plasticity model was tested in a simulation of an impacting glass sphere onto a steel target. The numerically derived impact diameters for different velocities were then successfully compared to an analytical expression for impact diameters.

Due to the successful implementation of the different models, we are confident to simulate the abrasive process of flow machining at a microscopic level. For this, we have presented a first holistic simulation of the AFM process at grain scale, although we have restricted our simulations to the application of a newtonian fluid, so far. We have shown that a spherical abrasive particle is dragged along with the fluid and then interacts with the edge of a workpiece that is placed within the channel. Deburring effects due to plastic deformations and material removal are clearly discernible.
In the future, the simulations will be extended to more complex shaped abrasive particles and more realistic fluids, i.e. fluids showing a viscoelastic behavior. As a long term goal, optimal grain shapes and fluid properties depending on the desired final shape of the workpiece shall be identified.

Acknowledgments

This work was supported by the FhG Internal Programs under the Grant No. WISA 823 260. Furthermore, the authors would like to express their gratitude to Fraunhofer IKTS for providing the experimental data for the calibration of the viscoelastic fluid model.

References

[1] C. Nutto, C. Bierwisch, H. Lagger, and M. Moseler, "Towards simulation of abrasive flow machining," in 7^{th} *International SPHERIC Workshop proceeding*, 2012.

[2] N. Phan-Thien, "A nonlinear network viscoelastic model," *Journal of Rheology*, vol. 22, no. 3, pp. 259–283, 1978.

[3] M. Baumgaertel and H. H. Winter, "Determination of discrete relaxation and retardation time spectra from dynamic mechanical data," *Rheologica Acta*, vol. 28, no. 6, pp. 511–519, 1989.

[4] M. Ellero and R. I. Tanner, "Sph simulations of transient viscoelastic flows at low reynolds number," *Journal of Non-Newtonian Fluid Mechanics*, vol. 132, no. 13, pp. 61 – 72, 2005.

[5] B. Corbett, "Numerical simulations of target hole diameters for hypervelocity impacts into elevated and room temperature bumpers," *International Journal of Impact Engineering*, vol. 33, no. 112, pp. 431 – 440, 2006, hypervelocity Impact Proceedings of the 2005 Symposium.

[6] T. Børvik, O. S. Hopperstad, T. Berstad, and M. Langseth, "A computational model of viscoplasticity and ductile damage for impact and penetration," *European Journal of Mechanics - A/Solids*, vol. 20, no. 5, pp. 685 – 712, 2001.

[7] M. Takaffoli and M. Papini, "Material deformation and removal due to single particle impacts on ductile materials using smoothed particle hydrodynamics," *Wear*, vol. 274-275, no. 0, pp. 50 – 59, 2012.

[8] G. R. Johnson and W. H. Cook, "A constitutive model and data for metals subjected to large strains, high strain rate, and temperatures," *in: International Symposium on Ballistics*, pp. 1–7, 1983.

[9] T. Mezger, *The rheology handbook: for users of rotational and oscillatory rheometers*, 3rd ed., ser. Coatings Compendien. Vincentz Network, 2011.

[10] A. W. Lees and S. F. Edwards, "The computer study of transport processes under extreme conditions," *Journal of Physics C: Solid State Physics*, vol. 5, no. 15, p. 1921, 1972.

[11] A. Harsha and D. K. Bhaskar, "Solid particle erosion behaviour of ferrous and non-ferrous materials and correlation of erosion data with erosion models," *Materials & Design*, vol. 29, no. 9, pp. 1745 – 1754, 2008.